J Mater Sci: Mater Med (2010) 21:3077–3083
DOI 10.1007/s10856-010-4161-y

Nano-hydroxyapatite/poly(L-lactic acid) composite synthesized by a modified in situ precipitation: preparation and properties

C. Y. Zhang · H. Lu · Z. Zhuang · X. P. Wang · Q. F. Fang

Received: 3 September 2009 / Accepted: 21 September 2010 / Published online: 2 October 2010

Abstract Nano-hydroxyapatite/poly(L-lactic acid) (nano-HA/PLLA) composites with uniform HA distribution and good mechanical performance were fabricated by a modified in situ precipitation method, using $Ca(OH)_2$ and H_3PO_4 as precursors for the synthesis of HA phase. This method has solved the aggregation problem of the nano-sized particles in the polymer matrix. The X-ray diffraction, Fourier transform infrared spectroscopy, and transmission electron microscopy were used to characterize the phase composition, chemical interactions and morphology of the composites, while the mechanical properties were determined by compressive measurements. The results show that the rod-like nano-HA particles synthesized by this method were uniformly distributed in the PLLA matrix. The compressive strength and Young's modulus of the composites were greatly enhanced and reached the values of 155 MPa and 3.6 GPa at 20 wt% HA content, respectively, which are much higher than those of the reference samples fabricated by direct mixing of PLLA with nano-HA particles. This supports the potential of these composites for applications in bone tissue engineering and load bearing bone defects repair.

C. Y. Zhang · H. Lu · Z. Zhuang · X. P. Wang · Q. F. Fang (✉)
Key Laboratory of Materials Physics, Institute of Solid State Physics, Chinese Academy of Sciences, Hefei 230031, People's Republic of China
e-mail: qffang@issp.ac.cn

C. Y. Zhang
School of Pharmacy, Anhui Traditional Chinese Medical College, Hefei 230038, People's Republic of China

1 Introduction

Bones are rigid organs with the microstructure that is hierarchically patterned to provide maximal strength with minimal mass. Many circumstances call for bone grafting, which is due to bone defects deriving from traumatic or non-traumatic destructions [1]. A few therapies are clinically available for the treatment of bone defects, but there exist disadvantages, such as donor shortage, a chance for rejection, and a risk of transmission of infectious disease. In this context there is an ongoing search in the field of bone repair for new biomaterials that are biocompatible, biodegradable to nontoxic products, osteoinductive, osteoconductive, and have composition and mechanical properties similar to natural bones [2–30].

Hydroxyapatite (HA) has now been recognized as a promising bone substitute, which is mainly due to its chemical and biological similarities to the mineral phase of the native bones. In addition, HA possesses good biocompatibility, osteoconductivity and bone-bonding properties [4–10]. However, the brittleness of HA ceramics limits its clinical application to repairs of load-bearing bones [11]. By contrast, biodegradable polymers such as poly(lactic acid) (PLA), poly(L-lactic acid) (PLLA), poly(glycolic acid) (PGA), and poly(D,L-lactic acid-co-glycolic acid) (PLGA) are biomaterials that are ductile, and their properties have been exploited in the fabrication of scaffolds for cell transplantation and tissue engineering [12–15]. The osteoconductivity of calcium phosphates combined with the good workability of the polyesters gave rise to the development of a variety of bio-ceramic/polyester composite scaffolds for bone tissue engineering [16, 17]. For the same reason hydroxyapatite/poly(L-lactic acid) (HA/PLLA) nano-composites have received attention in orthopedic and dental applications.

A critical factor that determines the properties of HA/PLLA composites is a fine dispersion of HA filler in the PLLA matrix. The issue has not been satisfactorily solved up to date [18]. Mechanical [19–22] and ultrasonic stirring [23] have been used to enhance the fine distribution of HA particles in the matrix. The effects, however, are temporary and without stirring the particles tend to re-aggregate. In an attempt to synthesize the HA/PLLA composites with uniform distribution of HA particles, various modification methods have been proposed in the past decade [17, 24–29]. Most of these modifications, however, were carried out on the surface of ex-situ grown HA particles that were already agglomerated. Moreover, many organic compounds used for HA grafting are usually noxious. Tian et al. [30] on the other hand, have fabricated HA/PLLA composite by infiltrating PLLA into the framework of sintered HA. Sintered apatite, however, rarely remolds in vivo, which is due to its high crystallinity.

The aim of this study was to obtain nano-HA/PLLA composites with uniform nano-HA dispersion and good mechanical properties. We mimicked the natural bone formation by using a bionic approach that consists of the modified in situ precipitation method [31–33]. In the method nano-HA particles were synthesized in situ using $Ca(OH)_2$ and H_3PO_4 as precursors in the PLLA template and biocompatible PEG was added to improve the interface adhesion between HA and PLLA. In order to evaluate the effect of nano-HA particle incorporation on the properties of HA/PLLA composites, compressive measurements were performed on the particulate reinforced composites obtained by hot pressing.

2 Materials and methods

$Ca(OH)_2$, H_3PO_4, polyethylene glycol (PEG 2,000) and *N*,*N*-dimethyl formamide (DMF), all of AR grade, were purchased from Sinopharm Chemical Reagent Co., Ltd., P.R. China, and poly-L-lactic acid (Mw 200,000), from Shengzhen BrightChina Industrial Co., Ltd., P.R. China.

2.1 Synthesis of pure nano-HA particles

Pure nano-HA particles were synthesized by wet chemical method from $Ca(OH)_2$ and H_3PO_4 along the following equation [34]:

$$10Ca(OH)_2+6H_3PO_4 \rightarrow Ca_{10}(PO_4)_6(OH)_2+18H_2O \quad (1)$$

With the atomic ratio Ca/P $\approx$ 1.67, an appropriate amount of 0.6 mol/l H_3PO_4 aqueous solution was slowly titrated into the mixture that contained 0.025 mol/l $Ca(OH)_2$ and 71.4 vol.% DMF at 80°C under continuous stirring, while the pH value of the mixture was adjusted to be about 10. After the titration, the precipitate was aged at room temperature for 24 h. The nano-HA particles were obtained by washing the precipitate with deionized water and drying at 100°C.

2.2 Fabrication of nano-HA/PLLA composites by in situ precipitation

Prior to the synthesis of the composite, 0.6 mol/l H_3PO_4 in DMF was added drop-wise into 50 g/l PLLA in DMF with continuous stirring to get a homogeneous solution. At the same time, an appropriate amount of PEG 2000 aqueous solution was added to the mixture of 0.025 mol/l $Ca(OH)_2$ and 71.4 vol.% DMF solution. To fabricate the composite, the two solutions were slowly titrated into 200 ml DMF at 80°C at the atomic ratio of Ca/P $\approx$ 1.67. The titration speed was controlled to maintain the pH at about 10. The resultant solution turned blue at the end of the titration process. After stirring for 2 h and aging for 12 h at room temperature, the deionized water was added to make the HA and PLLA co-precipitate. Finally, the nano-HA/PLLA composite was obtained by washing the precipitate three times with deionized water and drying at 48°C.

The composites were prepared at the following HA/PLLA weight ratios: 5/95, 10/90, 15/85, 20/80, and 25/75. The initial amounts of the reagents used are listed in Table 1. Samples with higher HA content were not prepared, which is because PLLA degrades at high H_3PO_4 and $Ca(OH)_2$ concentrations.

For comparison, another kind of nano-HA/PLLA composite with the same HA weight content was prepared by direct mixing the synthetic nano-HA with PLLA DMF solution.

2.3 Characterization

The phase composition was identified by X-ray diffraction (XRD) in a Philips X'pert PRO X-ray diffractometer with Cu–Kα radiation. The XRD patterns were collected at room temperature in the 2θ scanning range from 10° to 70° with a step of 0.033° and a scanning rate of 10.16 s per step. The Fourier transform infrared (FT-IR) spectroscopy measurements were used to confirm the chemical

Table 1 The dosage of reagents for the preparation of nano-HA/PLLA composites

Nano-HA/PLLA composite (wt%)	PLLA (g)	$Ca(OH)_2$ (g)	H_3PO_4 (g)
5/95	9.5	0.37	0.294
10/90	9	0.74	0.588
15/85	8.5	1.11	0.882
20/80	8	1.48	1.176
25/75	7.5	1.85	1.470

composition and possible chemical interactions between HA and PLLA in the composites. All samples for FT-IR measurements were mixed with KBr powders and then pressed into the discs. The FT-IR spectra were recorded from 4000 to 400 cm^{-1} with a Nicolet Nexus spectrometer operating in transmission mode. Transmission electron microscopy (TEM) was employed to characterize the morphology of both the HA particles and the nano-composites. TEM images were taken with a JEOL-2010 microscope and the samples were prepared by dripping a drop of the ethanol suspension of the composites onto a TEM grid covered with a carbon film and by evaporating the solvent completely at room temperature. Energy dispersive spectroscopy (EDS, Oxford INCA) was implemented to estimate the atomic proportion of Ca and P in the HA particles.

Mechanical properties of the nanocomposite were evaluated by compressive measurements with a CMT4204 mechanical tester (SANS, China) at a maximum load of 20 kN. The samples for compressive tests were prepared as follows. The powders of the HA/PLLA composites were placed in a cylindrical stainless steel mould with an internal radius of 10 mm, then preheated at 145°C for 30 min, and pressed for 2 min under a pressure of 200 MPa. The length of the cylindrical hot pressed samples was about 20 mm. The cross-head speed was set as 1 mm/min, and the load was applied until the specimen was crushed. The elastic modulus was calculated as the slope of the initial linear part of the stress–strain curve. When the yield point was not clear, the yield stress was determined from the cross point of the two tangents on the stress–strain curve (Fig. 4). The data for compressive strength and Young's modulus are the averages of at least five measurements.

3 Results and discussion

3.1 XRD results

Figure 1 shows the XRD patterns recorded for the pure PLLA (curve a), the inorganic component obtained by burning out the organic materials in the composite (curve b), the nano-HA/PLLA composite (curve c), and the pure nano-HA (curve d). As can be seen, the XRD pattern of the pure PLLA exhibits two characteristic peaks around $2\theta = 17^{o}$ and 19^{o}. The peaks at $2\theta = 25.9°$, 31.9°, 33.2°, 34.2°, 35.1°, and 40.1° detected in the patterns of the pure nano-HA and of the inorganic component in the composite can be well indexed as those of the HA phase (JCPDS card 09-432 [35]). This illustrates that the HA particles synthesized in this study are a pure phase. By contrast, the XRD pattern of the nano-HA/PLLA composite (curve c) consists of the same peaks characteristic of the pure HA

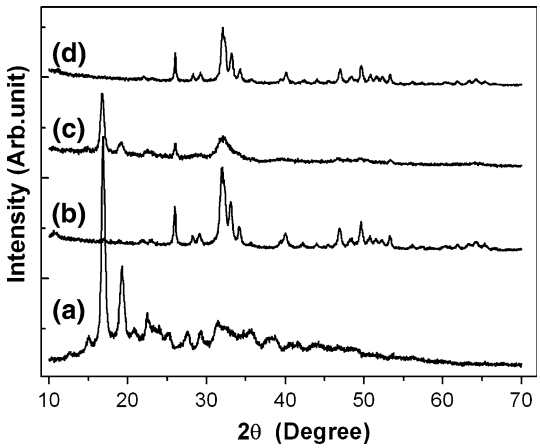

Fig. 1 XRD patterns of (*a*) pure PLLA, (*b*) the inorganic component obtained by burning out the organic materials in the composite, (*c*) the nano-HA/PLLA composite, and (*d*) nano-HA

and PLLA phases, however, with a larger width at half maximum. This implies the existence of smaller crystallites in the composites. According to the Scherrer equation, the crystallite size of pure HA particles and the HA particle in the composites is 41 and 27 nm, respectively. By comparing the XRD patterns of the nano-HA/PLLA composite (curve c) with those of the pure HA (curve b or d) and the pure PLLA (curve a), it can be seen that the crystallinity of HA and PLLA in the composites is obviously lower, indicating that there may exist PLLA-nano-HA interactions. These crystallographic characteristics of HA synthesized in this study are similar to those of the mineral (biological apatite) in natural bones [36].

In the nano-HA/PLLA composites synthesized in this work, the nucleation and growth of HA crystallites were restrained by the PLLA matrix. On the other hand, the inorganic nano-particles could inhibit somewhat the crystallization of PLLA. Therefore, the crystallite size of HA in the composites is smaller than that of the pure nano-HA particles and the crystallinity of both HA and PLLA in the composites is lower than when the compound was synthesized independently.

3.2 FT-IR results

FT-IR spectra of the nano-HA/PLLA composite, the nano-HA, and the pure PLLA are shown in Fig. 2. It follows from the spectra that the composite consists of HA and PLLA. In the spectrum of the nano-HA (c), the absorption bands at 1092, 1035, 961, 602 and 567 cm^{-1} correspond to different vibration modes of PO_4^{3-}, while those at 3571 and 630 cm^{-1} can be assigned to the stretching and bending vibration of OH^{-}. The fact that these characteristic bands also exist in the FT-IR spectra of the bone apatite [37] suggests the similarity of the nano-HA crystallites synthesized in this study to the

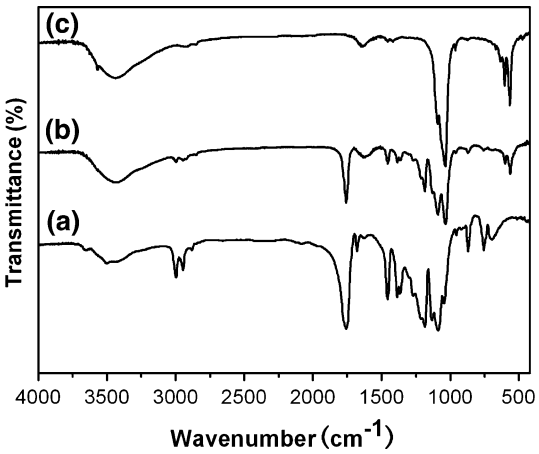

Fig. 2 FT-IR spectra of (*a*) pure PLLA, (*b*) 10 wt% nano-HA/PLLA composite, and (*c*) pure nano-HA

bone apatite. Furthermore, a lower intensity of OH^- absorption bands and carbonyl (C=O) stretching vibration bands in the spectrum of the nanocomposite may be indicative of the formation of hydrogen bonding between the OH^- group of the nano-HA and the functional groups of PLLA. In addition, a slight shift and a decrease in intensity of the C–H vibration bands together with the disappearance of carboxyl groups (–COOH) absorbance bands in the spectrum of the nanocomposite also suggest the occurrence of possible molecular interactions between the nano-HA and PLLA in the nanocomposite. These interactions may greatly affect the interfacial behavior and mechanical properties of the composites.

3.3 Microscopy

Figure 3 presents TEM images of 10 wt% nano-HA/PLLA composite (Fig. 3a) and of the nano-HA crystallites (Fig. 3b) with EDS spectrum (Fig. 3c). The images of the other samples were similar and are not shown. Figure 3a reveals that the nano-scaled HA particles are distributed homogeneously in the PLLA matrix and that the interface between the nano-HA crystallites and the PLLA is closely compacted. The rod-like HA crystallites are about 10–30 nm in diameter and 40–100 nm in length (Fig. 3b). The molar ratio of Ca/P in the synthesized nano-HA particles was deduced as 1.6 from the EDS spectra, which is close to the stoichiometric composition of HA (Ca/P $\approx$ 1.67). Thus, it is worth noting that the particle size and the elemental composition of the prepared nano-HA crystallites are similar to the apatite phase in the natural bones [37]. Importantly, it can be expected that the uniform distribution of the nano-HA in the nano-HA/PLLA composite powders

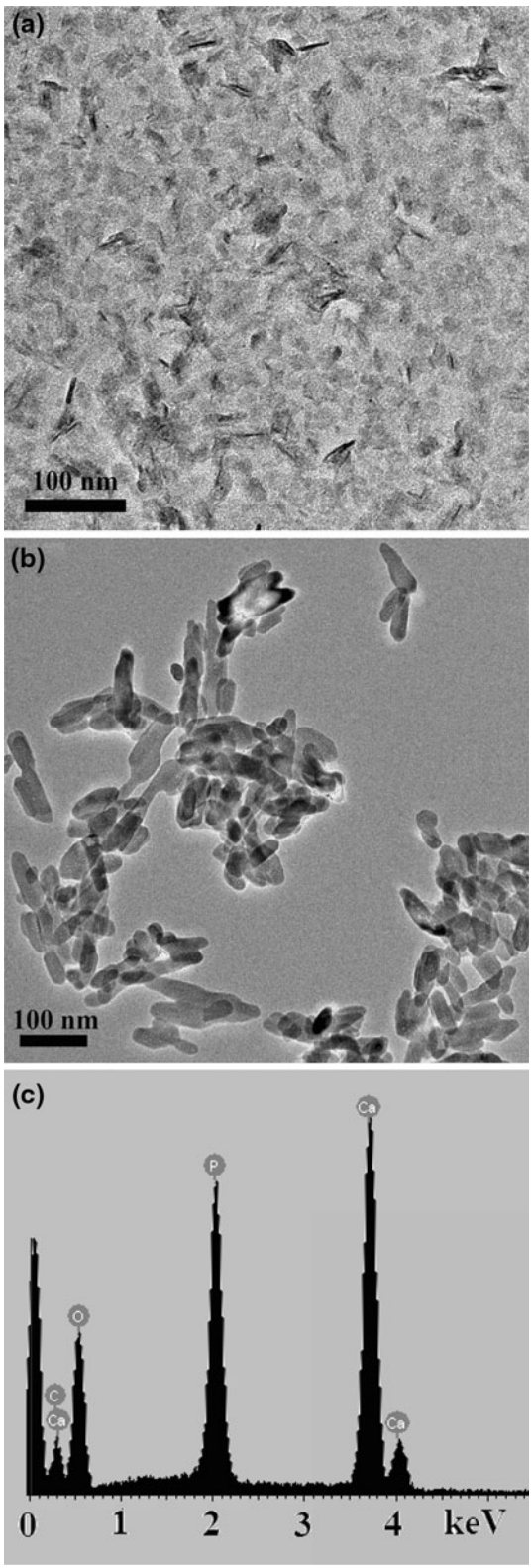

Fig. 3 TEM micrographs of **a** 10 wt% nano-HA/PLLA composite, and **b** pure nano-HA with EDS spectrum (**c**)

guaranties a fine distribution of the nano-HA in the bulk products manufactured from these composite powders.

3.4 Mechanical properties

The mechanical properties of the nano-HA/PLLA composites were evaluated from the compressive stress–strain measurements. The results for different nano-HA content in the composites are shown in Fig. 4. It is worth pointing out that the presence of HA nano-crystallites influences the fracture mode of the nano-composites. The nano-HA/PLLA composites exhibit rupture behavior between plastic deformation and brittle fracture, while the pure PLLA samples exhibit uniform plastic deformations without any rupture.

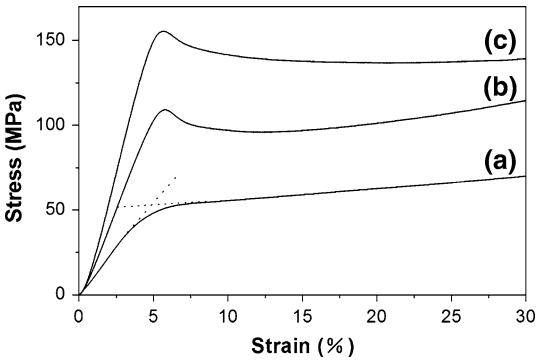

Fig. 4 Curves of compressive stress versus strain for three different nano-HA contents: (*a*) pure PLLA, (*b*) 10 wt% HA, and (*c*) 20 wt% HA

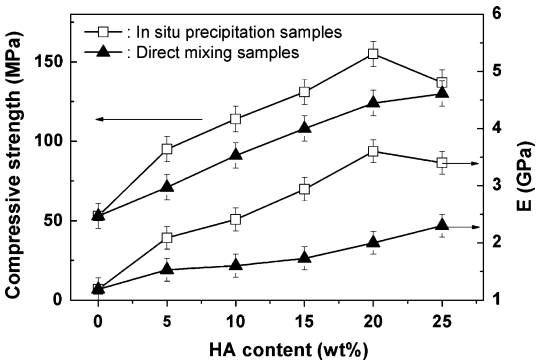

Fig. 5 Dependence of compressive strength and Young's modulus on the nano-HA content in nano-HA/PLLA composites fabricated by in situ precipitation and by direct mixing method, respectively

Compressive strength and Young's modulus are presented in Fig. 5 as a function of HA content in the nano-HA/PLLA composites. The results of the samples prepared by direct mixing are also shown for comparison. From the obtained mechanical data it can be inferred that the incorporation of HA into PLLA matrix resulted in a significant enhancement of the mechanical properties. When the HA content increases from 0 to 20 wt%, the compressive strength and Young's modulus of the composites increase monotonously from 53 MPa to 155 MPa and from 1.2 to 3.6 GPa, respectively. Furthermore, these values are definitely higher than those of the samples prepared by direct mixing. The observed difference in the mechanical properties of these two kinds of composites may thus be viewed as resulting partly from the molecular interactions between PLLA and HA in the in situ precipitated composites, which was confirmed by the XRD and FT-IR results (Sects. 3.1 and 3.2), and partly from the more uniform distribution of the nano-HA particles. As shown in Table 2, when compared to the nano-HA/PLLA composites reported in the literature [38–40], the nano-HA/PLLA composites prepared by the in situ precipitation in this study have superior mechanical properties. However, with a further increase in HA content, the compressive strength and Young's modulus slightly decreased, which may be a result of the PLLA degradation at high H_3PO_4 and $Ca(OH)_2$ dosage.

The primary problem during the development of bone substitutes is how to obtain homogeneous composites with the mechanical properties comparable with the natural bone tissue. It was reported that the compressive strength and elastic modulus of the natural bone vary, for instance

Table 2 Compressive strength and Young's modulus of dense HA/PLLA composites

Method	Tested materials			Mechanical properties	
	Molecular weight (PLLA) (kDa)	Filler (HA) characteristics (content, size)	Processing conditions	Compressive strength (MPa)	Elastic modulus (GPa)
This work	200	10 wt%, 40–100 nm	145°C, 200 MPa	109 ± 8	2.3 ± 0.2
		20 wt%, 40–100 nm		155 ± 8	3.6 ± 0.2
[38]	104	25 wt%, 100 nm	190°C, 300 MPa	88	3.8
		50 wt%, 70–100 nm		97	5.6
[39]	100	80 wt%, 0.5–0.7 mm	176°C, 98 MPa	38	2.0
		80 wt%, 100 nm		72	3.5
[40]	202	50 wt%, 0.3–20 μm	103°C	115	6.5

for the load bearing bone tissue the former amounts to between 1.9 and 167 MPa, and the latter to between 0.09 and 18.6 GPa [41]. In this work the compressive strength up to 155 MPa and elastic modulus up to 3.6 GPa were measured for the nano-HA/PLLA composites containing 20 wt% HA obtained by the in situ precipitation. The values correspond to the top values of the ranges for the natural load bearing bone, thus making the composites a promising candidate for bone tissue engineering.

4 Conclusion

In this study the nano-HA/PLLA composites were fabricated by a modified in situ precipitation method. These composites mimic natural bones in such aspects as crystallinity, elemental composition, crystallite size, and fine distribution of HA crystallites in the polymer matrix. The compressive strength and Young's modulus of the composites were found to be high. These features may be explained by both molecular interactions between the nano-HA particles and the PLLA matrix and the uniform distribution of the nano-HA particles in the composites. The experimental results demonstrate the feasibility of this bionic approach for the preparation of the nano-HA/PLLA composites with excellent performance. The resultant nanocomposites are promising biomedical materials that may be applied in load bearing bone repair and bone tissue engineering.

Acknowledgment The authors wish to thank Dr. Chun Li at Nanchang Hangkong University for her help in the compression experiments.

References

1. Murugan R, Ramakrishna S. Development of nanocomposites for bone grafting. Compos Sci Technol. 2005;65:2385–406.
2. Kusmanto F, Walker G, Gan Q, et al. Development of composite tissue scaffolds containing naturally sourced microporous hydroxyapatite. Chem Eng J. 2008;139:398–407.
3. Gunatillake PA, Adhikari R. Biodegradable synthetic polymers for tissue engineering. Eur Cells Mater. 2003;5:1–16.
4. Hench LL, Wilson J. Surface-active biomaterials. Science. 1984; 226:630–6.
5. Hardy DCR, Frayssinet P. Osteointegration of hydroxyapatite coated stems of femoral prostheses. Eur J Orthop Surg Traumatol. 1999;9:75–81.
6. Shackelford JF. Bioceramics-current status and future trends. Mater Sci Forum. 1999;293:99–106.
7. Ducheyne P. Bioceramics—material characteristics versus in vivo behavior. J Biomed Mater Res Appl Biomater. 1987;21: 219–36.
8. Heise U, Osborn JF, Duwe F. Hydroxyapatite ceramic as a bone substitute. Int Orthop. 1990;14:329–38.
9. Kitsugi T, Yamamuro T, Nakamura T, et al. 4 calcium phosphate ceramics as bone substitutes for non-weight-bearing. Biomaterials. 1993;14:216–24.
10. Best S, Bonfield W. Processing behavior of hydroxyapatite powders with contrasting morphology. J Mater Sci: Mater Med. 1994;5:516–21.
11. Cleries L, Fernandez Pradas JM, Morenza JL. Behavior in simulated body fluid of calcium phosphate coatings obtained by laser ablation. Biomaterials. 2000;2:1861–5.
12. Zhang RY, Ma PX. Poly(alpha-hydroxyl acids)/hydroxyapatite porous composites for bone tissue engineering. I. Preparation and morphology. J Biomed Mater Res. 1999;44:446–55.
13. Maquet V, Jerome R. Design of macroporous biodegradable polymer scaffolds for cell transplantation. Mater Sci Forum. 1997;250:15–42.
14. Rose FR, Oreffo RO. Bone tissue engineering: hope vs hype. Biochem Biophys Res Commun. 2002;292:1–7.
15. Oh SH, Kang SG, Kim ES, Cho SH, Lee JH. Fabrication and characterization of hydrophilic poly(lactic-*co*-glycolic acid)/poly(vinyl alcohol) blend cell scaffolds by melt-molding particulate-leaching method. Biomaterials. 2003;24:4011–21.
16. Zhang RY, Ma PX. Porous poly(L-lactic acid)/apatite composites created by biomimetic process. J Biomed Mater Res. 1999;45: 285–93.
17. Qiu XY, Hong ZK, Hu JL, et al. Hydroxyapatite surface modified by L-lactic acid and its subsequent grafting polymerization of L-lactide. Biomacromolecules. 2005;6:1193–9.
18. Plueddemann EP. Silane coupling agents. 2nd ed. New York: Plenum Press; 1991.
19. Sada E, Kumazawa H, Murakami Y. Hydrothermal synthesis of crystalline hydroxyapatite ultrafine particles. Chem Eng Commun. 1991;103:57–64.
20. Ignjatovic N, Uskokovic D. Synthesis and application of hydroxyapatite/polylactide composite biomaterial. Appl Surf Sci. 2004; 238:314–9.
21. Kasuga T, Maeda H, Kato K, et al. Preparation of Poly(lactic-acid) composites containing calcium carbonate. Biomaterials. 2003;24:3247–53.
22. Nikcevic I, Maravic D, Ignjatovic N, et al. The formation and characterization of nanocrystalline phases by mechanical milling of biphasic calcium phosphate/poly-L-lactide biocomposite. Mater Trans. 2006;47:2980–6.
23. Fang Y, Agrawal DK, Roy DM, et al. Ultrasonically accelerated synthesis of hydroxyapatite. J Mater Res. 1992;7:2294–8.
24. Borum-Nicholas L, Wilson OC. Surface modification of hydroxyapatite. Part I. Dodecyl alcohol. Biomaterials. 2003;24:3671–9.
25. Liu Q, Wijn JR, Bakker D, et al. Polyacids as bonding agents in hydroxyapatite polyester-ether (polyactive (TM) 30/70) composites. J Mater Sci: Mater Med. 1998;9:23–30.
26. Wang XJ, Li YB, Wei J, Groot K. Development of biomimetic nano-hydroxyapatite/poly (hexamethylene adipamide) composites. Biomaterials. 2002;23:4787–91.
27. Dong GC, Sun JS, Yao CH, Jiang GJ, Huang CW, Lin FH. A study on grafting and characterization of HMDI-modified calcium hydrogen phosphate. Biomaterials. 2001;22:3179–89.
28. Borum L, Wilson OC. Surface modification of hydroxyapatite. Part II. Silica. Biomaterials. 2003;24:3681–8.
29. Hong ZK, Qiu XY, Sun JR, Deng MX, Chen XS, Jing XB. Grafting polymerization of L-lactide on the surface of hydroxyapatite nano-crystals. Polymer. 2004;45:6699–706.
30. Tian T, Jiang DL, Zhang JX, Lin QL. Fabrication of bioactive composite by developing PLLA onto the framework of sintered HA scaffold. Mater Sci Eng C. 2008;28:51–6.
31. Li HY, Chen YF, Xie YS. Photo-crosslinking polymerization to prepare polyanhydride/needle-like hydroxyapatite biodegradable

nanocomposite for orthopedic application. Mater Lett. 2003;57: 2848–54.
32. Lin XY, Li XD, Fan HS, et al. In situ synthesis of bone-like apatite/collagen nano-composite at low temperature. Mater Lett. 2004;58:3569–72.
33. Murugan R, Ramakrishna S. In situ formation of recombinant humanlike collagen-hydroxyapatite nanohybrid through bionic approach. Appl Phys Lett. 2006;88:193124.
34. Lin FH, Yao CH, Huang CW, et al. The bonding behavior of DP-Bioglass and bone tissue. Mater Chem Phys. 1996;46:36–42.
35. Powder Diffraction File No. 9-432, International Centre of Diffraction Data (ICDD), Newton Square, PA, USA.
36. Li YB, Groot K, Wijn J, Klein CAPT, Meer SVD. Morphology and composition of nanograde calcium phosphate needle-like crystals formed by simple hydrothermal treatment. J Mater Sci: Mater Med. 1994;5:326–31.
37. Paschalis EP, Betts F, DiCarlo E, Mendelsohn R, Boskey AL. FTIR microspectroscopic analysis of normal human cortical and trabecular bone. Calcif Tissue Int. 1997;61:480–6.
38. Gay S, Arostegui S, Lemaitre J. Preparation and characterization of dense nano-hydroxyapatite/PLLA composites. Mater Sci Eng C. 2009;29:172–7.
39. Ignjatovic N, Delijic K, Vukcevic M, Uskokovic D. Microstructure and mechanical properties of hot-pressed hydroxyapatite/poly-L-lactide biomaterials. Bioceramics. 2000;192:737–40.
40. Shikinami Y, Okuno M. Bioresorbable devices made of forged composites of hydroxyapatite (HA) particles and poly-L-lactide (PLLA): part I. Basic characteristics. Biomaterials. 1999;20: 859–77.
41. Park J, Lakes R. Biomaterials-an introduction. 2nd ed. New York: Plenum Press; 1992. p. 7–316.